Supporting Information

Redox Regulation of $3d^0$ Ferrimagnetism in Pristine ZnO Nanofibres and Electrospinning Route of ZnO Porous Nanotubules

Authors' names and Institution

Jian-Min Li 🆔*, and Xian-Lin Zeng

Zhejiang Key Laboratory of Micro-Nano Quantum Chips and Quantum Control, School of Physics, Zhejiang University, Hangzhou 312007, China

ORCID ID Jian-Min Li: 0000-0002-3917-8653
*Email: phyjmli@zju.edu.cn

The thermal decomposition of the as-electronspun composites fibres was measured (Fig. S1) using a differential thermal analysis (DTA)-thermogravimetric analysis (TGA) (METTLER TOLEDO, TGA SDTA851). The morphology of nanofibers was characterized using scanning electron microscopy (SEM) and high-resolution transmission electron microscopy (HRTEM, FEI, 140 TECANAL G^2 F20 at an acceleration voltage of 200 kV). The microstructural characterized was made by powder X-ray diffraction results (PXRD, The PANalytical Empyrean Series 2 diffraction system), and Raman spectroscopy (Jobin Yvon HR-800 spectrometer, resolution of 1 cm^{-1}). The Raman experiments were carried out in a micro-Raman 180° backscattering geometry with 514.5 nm radiation from a 2-mW argon-ion laser at room temperature. In the experiment, the normalized photoluminescence (PL, Edinburgh Instruments FLS920, filter of 340 nm and resolution of 2.0 nm) spectra of stimulated emission were measured at room temperature to identify the defects states in ZnO with an excitation wavelength from a He–Cd laser at 325 nm. All magnetic measurements were performed using a Quantum Design MPMS XL-5 superconducting quantum interference device SQUID magnetometer. The X-ray photoelectron spectroscopy (XPS) measurements were performed using a VG ESCALAB 220IXL system with a monochromatic Al–K$_a$ X-ray source (1486.6 eV photons, background vacuum of 2×10^{-9} Pa).
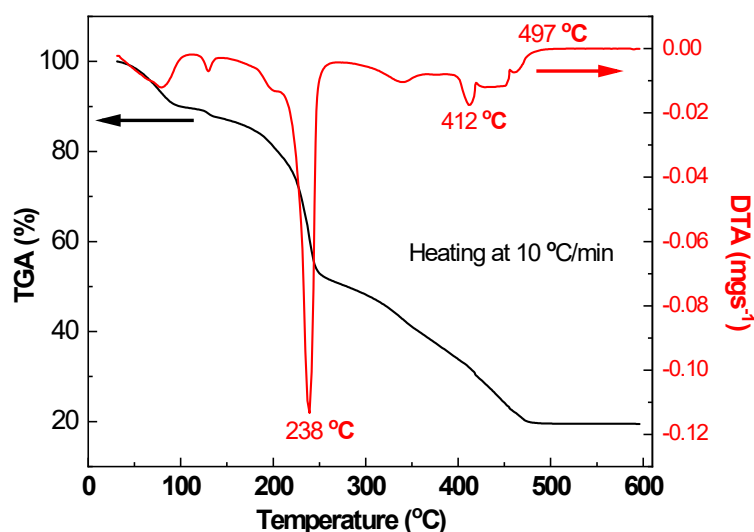
Figure S1. DTA-TGA curves of the as-electrospun PVA/ZnO-containing composite fibers in air. There are mainly two exothermic peaks in the DTA curve are observed at 238 °C (511 K), and 412 °C (685 K), respectively. The first sharp exothermic peak is responsible for the onset of PVA decomposition, and the second weak peak is crystallization of the ZnO, concurrent with a significant weight loss of about ~ 92.4 wt % takes place at 497 °C (770 K), indicating the complete removal of the organic component. As the decomposition temperature of PVA is relatively low (about 280 °C), PVA quickly decomposes, and has been completely decomposed at 550 °C.

Furthermore, a systematic and quantitative study on the effects of processing variables enables us to control the properties of electrospun ZnO NFs. The anneal processing was performed in a conventional horizontal tube furnace in flowing various atmospheres such as with hydrogen (H_2), oxygen (O_2), nitrogen (N_2), and ammonia (NH_3) gas, respectively. The neutral N_2 anneal was studied for comparison which is very similar to the as-synthesized (in air) electrospun ZnO NPMTs. The detailed results are summarized in Figs S2-S3. The nanosized ZnO powders were also prepared by means of the citrate–gel method and subsequently, after mechanically grinding using a mortar and pestle (Figure S7).
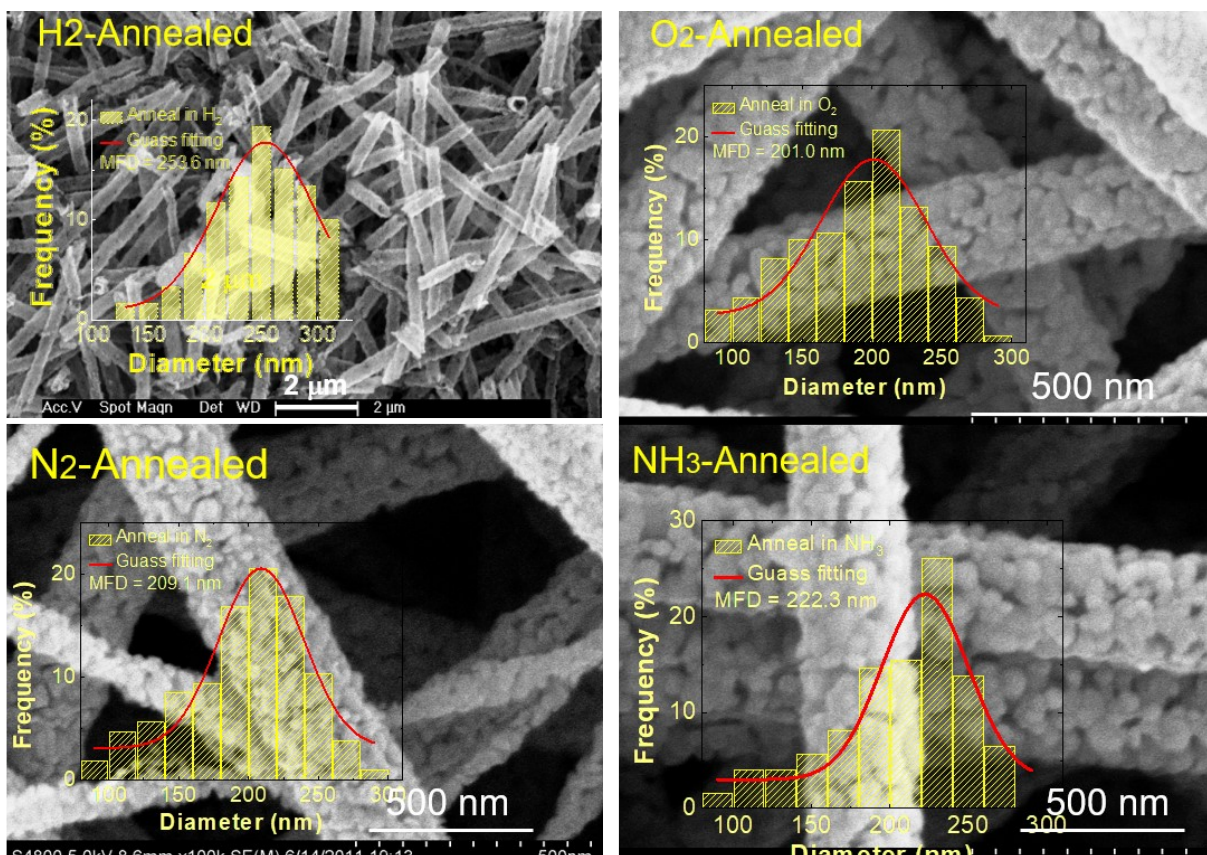
Figure S2. SEM images of as-calcined (in air) pristine as-synthesized ZnO NFs by post atmospheric anneals in H$_2$, O$_2$, N$_2$, and NH$_3$ anneal at 500 °C for 1 h. Insets, diameter distributions of ZnO NFs. The home-made vertical needle-collector electrospinning setup was given in [S1]
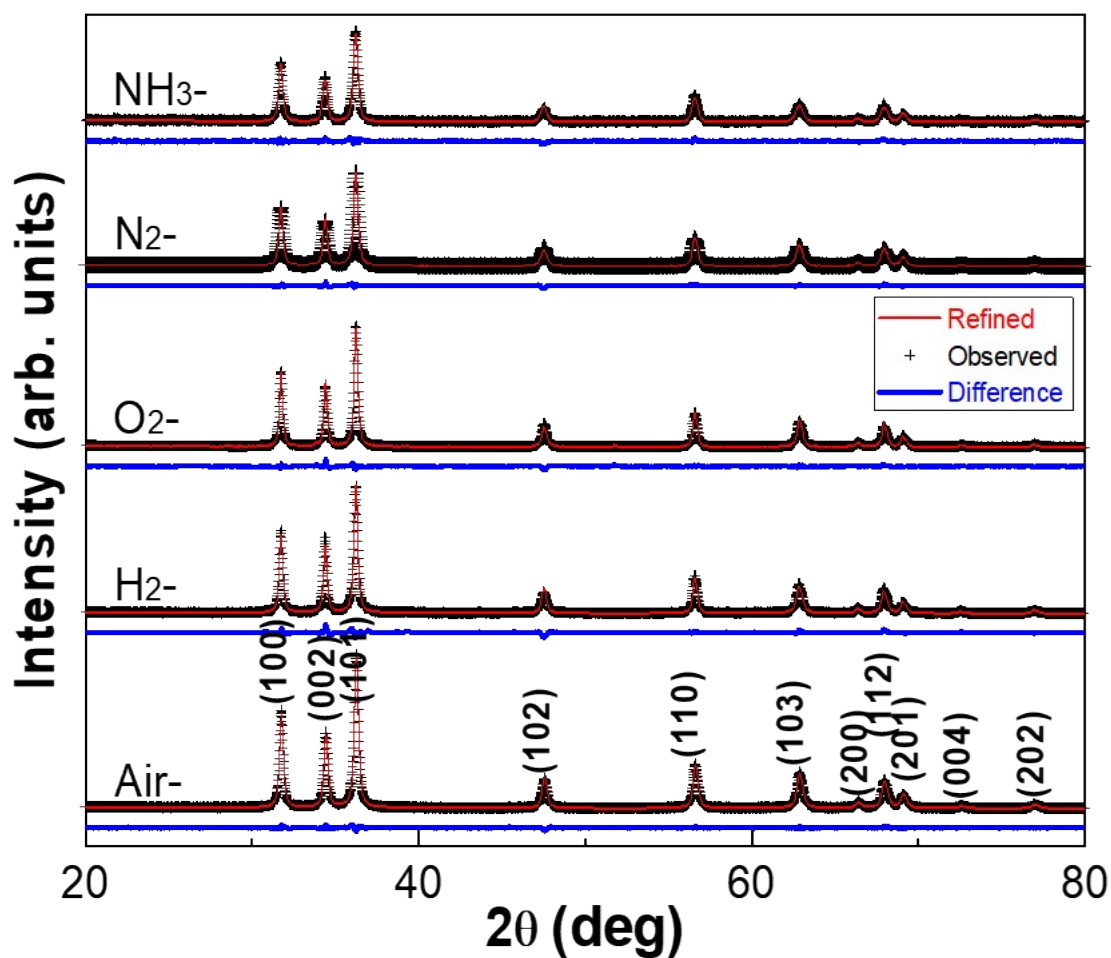
Figure S3. Powder X-ray diffraction (PXRD) patterns of as-calcined electrospun ZnO NFs by post atmospheric anneals in Air, H_2, O_2, and NH_3, and the corresponding Rietveld refinement profiles. All of the strong reflection peaks can be exactly indexed to hexagonal Wurtzite-structured ZnO (JCPDS 36--1451). All PXRD data are fitted by Rietveld refinement using RIETAN 2000 program, and the parameters obtained from PXRD are shown in Fig. S4.
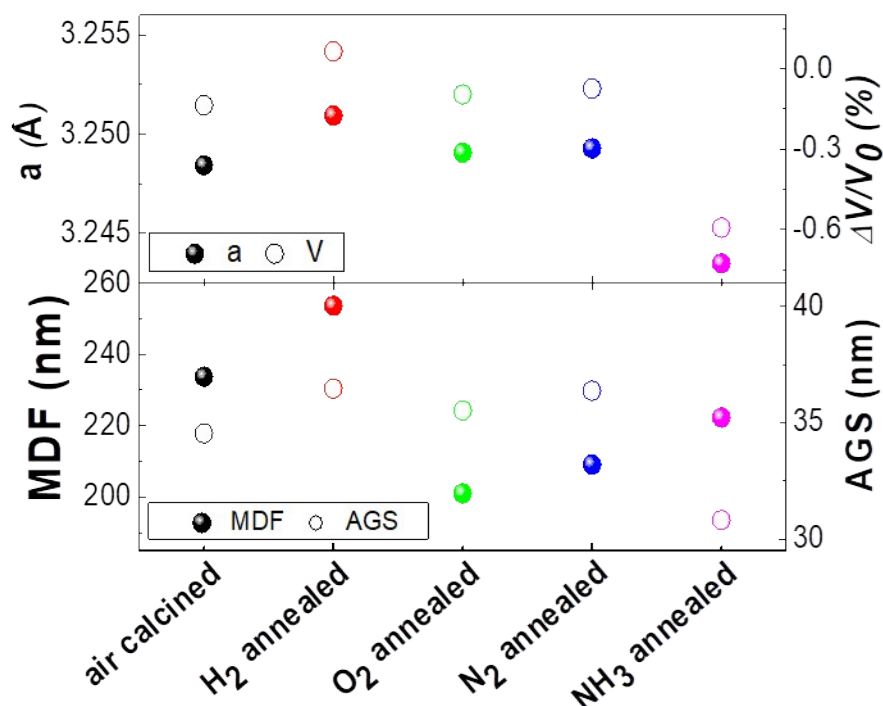
Figure S4. (Top) Dependence of lattice parameters (*a* and *c*), lattice cell, and (Bottom) mean fiber diameter (MFD) and average grain size (AGS) of as-calcined ZnO NFs by atmospheric anneals in Air, H_2, O_2, N_2, and NH_3. From the PXRD refinement results and the Williamson–Hall method, the lattice parameters (*a* and *c*) of the ZnO NFs by atmospheric anneals in Air, H_2, O_2, N_2, and NH_3. The lattice parameters average crystallite sizes of the ZnO NFs were estimated as shown in Fig. S4 (Top), which are similarly slightly larger than that of bulk ZnO (*a* = 3.24 Å and *c* = 5.19 Å), suggesting that lattice relaxation occurs. The average diameter of fiber (MFD) and average crystallite size (ACS) of the ZnO NFs was estimated as shown in Fig. S4 (Bottom).
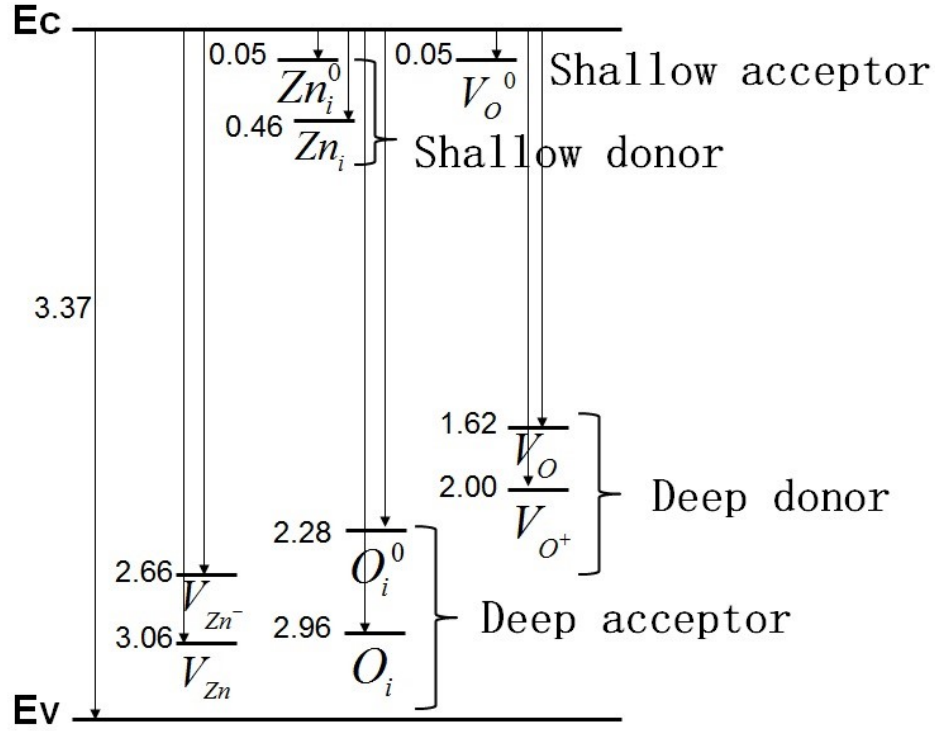
Figure S5. Energy level diagram of the ZnO. V_{Zn}, V_{Zn}^-, and V_{Zn}^{2-} denote neutral, singly charged, and doubly charged zinc vacancies, respectively. Shallow accepter (*SA*), shallow donor (*SD*), deep donor (*DD*, the dotted red arrow guides the eyes.). Zn_{io} and Zn_i indicate neutral zinc interstitials, while Zn^{i+} denotes a singly charged zinc interstitial. V_O^o and V_O denote neutral oxygen vacancies, while V_{O+} denotes a singly charged oxygen vacancy. O_i represents an oxygen interstitial. V_OZn^i denotes a complex of an oxygen vacancy and zinc interstitial. Singly negatively charged Zn vacancy (V_{Zn}^-).
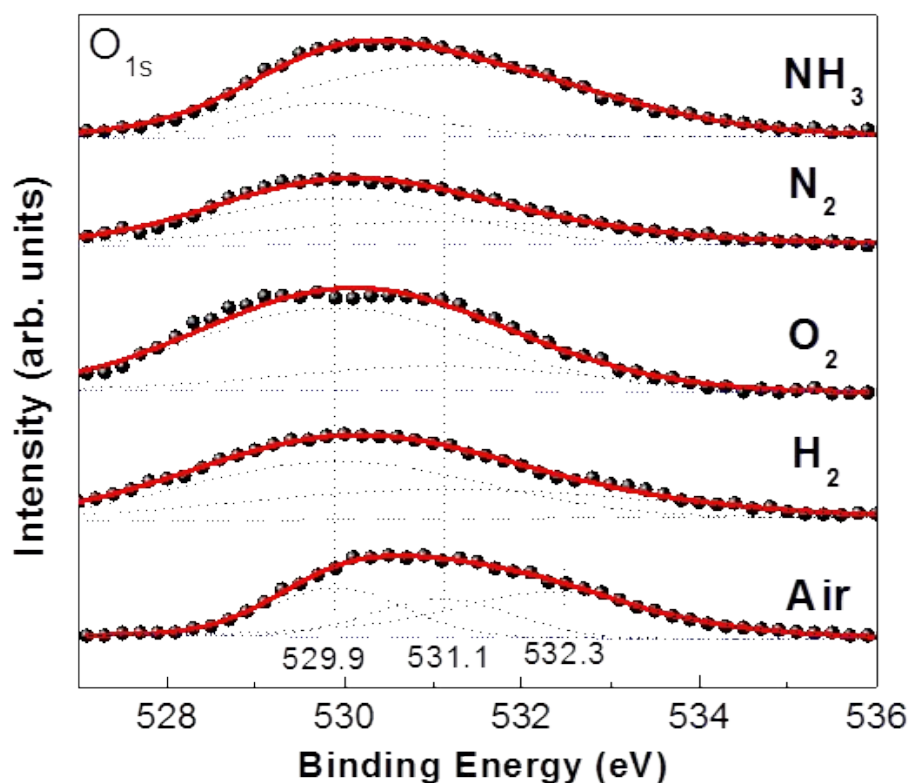
Figure S6. O1s core-level x-ray photoemission (XPS) spectra versus *x* in the as-calcined electrospun ZnO NFs in Air, H_2, O_2, N_2, and NH_3 annealing. The dotted lines guide the eyes.

XPS data confirmed N substitution at O site in ZnO NFs. The O*1s* peak fittings were fitted using two individual subpeaks at 531.1 eV (the dotted line guides the eyes), and 529.1 eV (the dotted line guides the eyes), respectively. The medium binding energy component, centered at 531.8 eV, is associated with O_2^- in the oxygen deficient regions with the matrix of ZnO [s2,s3]. It is believed that the intensity of this peak is connected to the variations in the concentration of oxygen vacancies. It suggests that the oxygen vacancies in ZnO samples were reduced when treated with high temperature annealing; this is consistent with the former conclusion and the Raman result. XPS was employed to detect the oxygen vacancy that O1s at 531.1 eV was considered as evidence of the Vo existence [s4-s6].
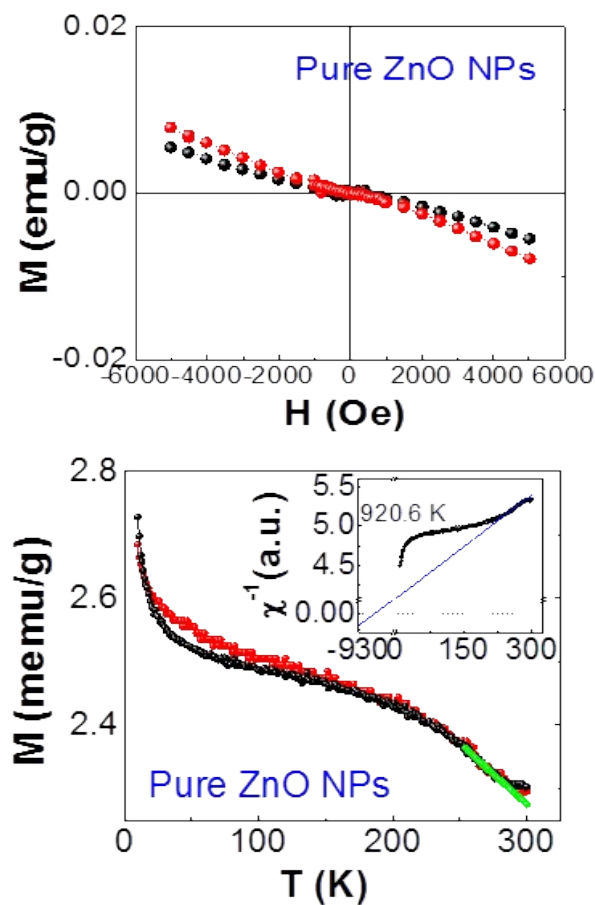
Figure S7. (top) The magnetization of the unelectrospun ZnO nanopowders (Fig.S4) at the same experimental conditions for comparison, and (bottom) Temperature-dependent magnetization ($M–T$) curves of undoped ZnO nanoparticles at a magnetic field of 1000 Oe. The black symbol, and red symbol represents zero-field cooling (ZFC), and field cooling (FC) susceptibility, respectively. The insets are the reciprocal magnetic susceptibilities (1/χ) vs T of undoped ZnO nanopowders (green regions, ZFC mode). Remarkably, ferromagnetism was never observed in zero-dimensional unelectrospun nanoparticles, and the nanocrystalline ZnO powders show more diamagnetic behavior, suggesting that the dimensional effect exists.

References

[S1] J. M. Li, X. L. Zeng, A. D. Mo, and Z. A. Xu. CrystEngComm. 13, 6964 (2011).

[S2] S. Park, T. Ikegami, K. Ebihara. Thin Solid Films 513, 90 (2006).

[S3] M. Chen, X. Wang, Y. H. Yu, Z. L. Pei, X. D. Bai, C. Sun, R. F. Huang, L. S. Wen. Appl. Surf. Sci. 158, 134 (2000).

[S4] V. G. Pol, R. Reisfeld, and G. A. Gedanken. Chem. Mater. 14, 3920 (2002).

[S5] J. M. Li, X. L. Zeng, Y. H. Dong, and Z. A. Xu. CrystEngComm. 15, 2372 (2013).

[S6] J. M. Li, Y. B. Hu. Appl. Phys. Lett. 114, 203101 (2019).